Journal of Materials Chemistry A

ROYAL SOCIETY OF CHEMISTRY

PAPER

View Article Online
View Journal | View Issue

Cite this: J. Mater. Chem. A, 2025, 13, 19007

One-pot scalable production of conjugated microporous polymers with exceptional functionality†

Duanlian Tang,‡[a] Zhuo Xiong, ‡[a] John D. Worth, [b] Ting Qiu,*[a] Charl F. J. Faul *[b] and Jie Chen *[a]

Conjugated microporous polymers (CMPs) are porous polymers that exhibit desirable functionality for a wide range of adsorption applications. Here, we report a one-step scalable approach that exploits moderately high temperature and pressure to overcome these limitations. Remarkably, this method achieves functional CMPs within 1 h with a specific surface area of 925 m^2 g^{-1}). Extending the reaction time to 5 h further enchances porosity to 1145 m^2 g^{-1}—a 20-fold improvement over conventional methods (58 m^2 g^{-1}). The original wide pore size distribution is refined to fall within a covalent organic framework (COF)-like microporous range, allowing the CMPs to function as versatile adsorbents for toxic mercury ions, achieving benchmark performance with an impressive capacity of 1429 mg g^{-1}, surpassing all previously reported materials. In addition, this approach features degas-free and facile scale-up opportunities, opening real possibilities for wide industrial applications of CMPs.

Received 3rd March 2025
Accepted 16th May 2025

DOI: 10.1039/d5ta01740h

rsc.li/materials-a

Introduction

Practical applications in sectors such as wastewater treatment necessitate advanced porous materials that possess high porosity, easy synthesis, and scalable production to ensure economic feasibility.[1–3] Recently, conjugated microporous polymers (CMPs) synthesized using the Buchwald–Hartwig (B–H) cross-coupling reaction have demonstrated significant advantages over other advanced porous materials.[4] These advantages are related to the high physical and chemical stability, abundant active N-heteroatom adsorption sites, novel pH-responsive doping–dedoping properties and thus the potential for fast adsorption–desorption kinetics.[5–9]

However, these CMPs, synthesized using expensive and rare-earth-containing palladium-based catalysts, face a significant technical challenge in that they are synthesized in scale-limited Schlenk lines or glove boxes under inert conditions due to the sensitivity of the palladium catalyst and base to moisture and oxygen.[10,11] Additionally, a successful synthesis generally takes 24–72 h or more due to the moderate reactivity, posing further significant hurdles to the industrial (adsorption) applications of these materials (Fig. 1(A and B)). Large-scale production of free-standing highly functional CMPs, with simple synthetic procedures, is therefore a significant hurdle to cross before widespread industrial exploitation of CMPs would be possible. In addition, B–H coupling usually produces CMPs with low yield, moderate porosity, and poor functionality. For example, the model sample of CMP, poly(triphenylamine) (PTPA) synthesized with standard procedures showed a low yield of 52% and specific surface area of 58 m^2 g^{-1}.[12,13] It also possesses unexpected broad pore size distribution (PSD) and low microporosity when compared with structurally related poly(-aryleneethynylene)s (PAEs, *e.g.*, CMP-1).[14,15] Although the previously developed Bristol–Xi'an Jiaotong (BXJ) approach[16,17] offers a methodology to address this issue, it still requires an oxygen-free environment for synthesis, particularly in B–H coupling applications. Additionally, it faces persistent challenges related to the scalability of synthesis processes.

To allow CMPs to be utilized in large-scale industrial adsorption applications, we report here a facile one-step, one-pot approach for the synthesis of palladium-catalyzed CMPs, which demonstrates significant improvements in porosity, functionality, and production scalability. Our approach uses a scalable autoclave approach to synthesize amorphous polymers simply and controllably by tuning the reactivity of monomers *via* the reaction temperature. This approach is anticipated to enhance reaction efficiency, porosity and functionality of CMPs. Additionally, we explore tuning the reaction conditions, including the vapor pressures of the moisture and oxygen in the reaction mixture (through the introduction of additional nitrogen (N_2) to the system) to remove the need for

[a]*Engineering Research Centre of Reactive Distillation, College of Chemical Engineering, Fuzhou University, Fuzhou 350108, P. R. China. E-mail: tingqiu@fzu.edu.cn; jiechen@fzu.edu.cn*

[b]*School of Chemistry, University of Bristol, Bristol, BS8 1TS, UK. E-mail: charl.faul@bristol.ac.uk*

† Electronic supplementary information (ESI) available. See DOI: https://doi.org/10.1039/d5ta01740h

‡ These authors contributed equally to this work.

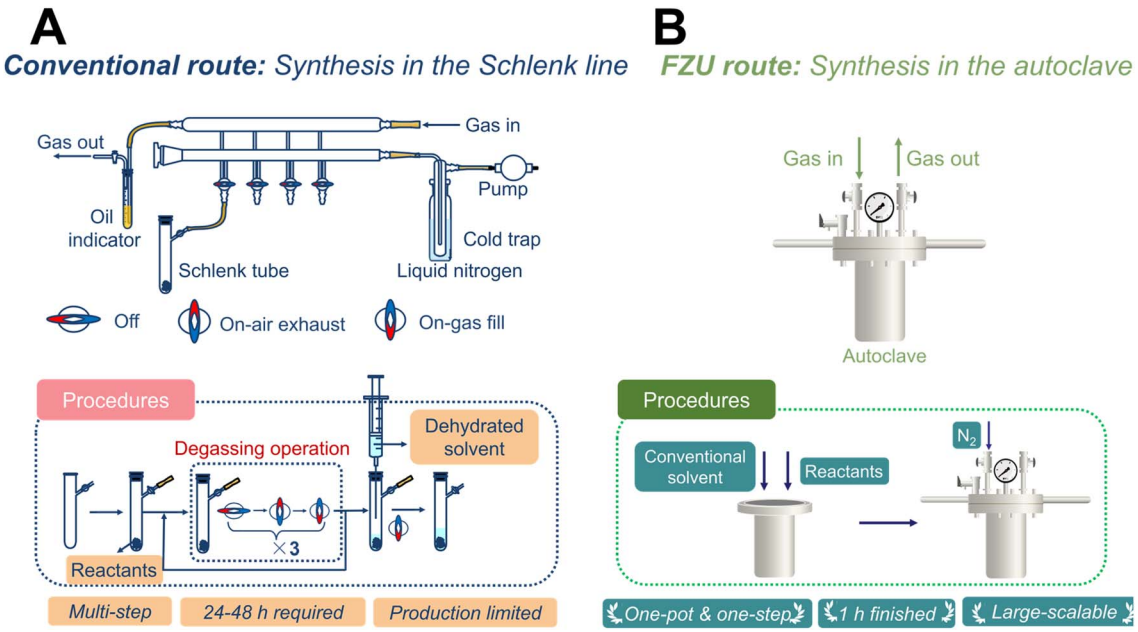

Fig. 1 Synthesis of PTPA by conventional or FZU route: (A) illustration of conventionally used Schlenk line and associated complicated synthesis procedures in the Schlenk line; (B) illustration of the autoclave in FZU route and the straightforward one-step synthesis procedure for FZU-PTPA in an autoclave.

tedious degassing procedures. We name this simple hydrothermal approach the Fuzhou University (FZU) approach, and note that this is the first study to show scalable synthesis of palladium-catalyzed CMPs. This facile one-step procedure has the potential to transition CMPs from the laboratory to industry in the very near future.

Results and discussion

We synthesized our model CMP-PTPA under hydrothermal conditions at a range of temperatures, from 80 °C (a temperature which is slightly higher than the boiling point of tetrahydrofuran (THF, 67 °C)) to 120 °C. The starting materials and solvent were directly added to the autoclave, with no procedures conducted for the removal of moisture and oxygen (Fig. 1(B)). We also shortened the reaction time to 5 h (compared with the conventional solvothermal method with a reaction time of 24–72 h, typically 48 h) to examine the reaction efficiency of our FZU methodology.

Encouragingly, as shown in Table 1, our approach immediately led to significantly improved yields (94.7% at 80 °C). Yields of PTPA could be further improved to 99% with increased temperatures (to 100 °C), representing a significant improvement from *ca.* 52.1% using the standard reaction conditions (Fig. 1(A and B)). More importantly, our FZU approach successfully produced *ca.* 2.0 g in a 100 mL autoclave (compared with *ca.* 400 mg in a Schlenk tube, Fig. 2(A)), highlighting opportunities for CMPs to be used in industrial applications.

We characterized both the control as well as the FZU-produced palladium-catalyzed CMPs using solid-state ^{13}C nuclear magnetic resonance (SS ^{13}C NMR) and Fourier-transform infrared (FTIR) spectroscopy. As shown in Fig. 2(B), the spectra confirmed the production of the desired PTPA polymer. The two main resonances at 144 and 128 ppm were ascribed to substituted phenyl carbons and unsubstituted phenyl carbons, respectively, fitting well with both the control and the calculated structures (as displayed in the ESI, Fig. S1†).[12] Successful coupling was also verified by FTIR spectroscopy (Fig. 2(C) & S2†), which confirmed the characteristic peaks assigned to the tris(4-bromophenyl)amine core and phenylenediamine linker. For example, the peaks attributed to the aniline groups, highlighted in blue, are clearly observed (see Fig. S3† for further details), whereas signals assigned to C–Br from the core (710, 1004 and 1070 cm^{-1}, highlighted in pink) and to $-NH_2$ from the linker (3400 and 3300 cm^{-1}, highlighted in purple) are absent.[18]

Next, we analyzed the porosities of these FZU-PTPAs by N_2 sorption isotherm studies to investigate the influence of the FZU approach on the porosities of PTPA. As shown in Fig. 2(D) and S5(a),† the conventionally synthesized PTPA showed a Type II sorption isotherm, with a very low adsorption of N_2 in the relative low-pressure area ($P/P_0 < 0.01$), indicating a low porosity and a correspondingly moderate specific surface area. Significantly, PTPAs from our FZU approach, exhibited a Type I sorption isotherm with a steep rise at low relative pressure, revealing the presence of micropores in these samples, before becoming more Type IV in nature at higher relative pressures.[19]

The Brunauer–Emmett–Teller (BET) specific surface areas were calculated to confirm the influence of the additional micropores (Table 1). Interestingly, the surface area of PTPA, with an initially low value of 58 $m^2\ g^{-1}$, was dramatically improved more than eleven times to 684 $m^2\ g^{-1}$ when the reaction temperature was slightly increased to 80 °C. The specific surface area was further increased *ca.* 20 times to 1145

Table 1 The reaction yields, porosity parameters, and gaseous CO_2 adsorption (273 K, 1 atm) performance of FZU-PTPAs synthesized under various conditions

Samples	Yield (%)	Surface area[a] ($m^2\ g^{-1}$)	Total pore volume[b] ($cm^3\ g^{-1}$)	Micropore volume ($cm^3\ g^{-1}$)	CO_2 uptake [c] (mmol g^{-1})
Control	52.1	58	0.066	0.046	0.91
BXJ-PTPA	99.2	1134	0.89	0.83	1.59
67 °C[d]	<1	N.A.	N.A.	N.A.	N.A.
80 °C[d]	94.7	684	0.36	0.22	2.56
90 °C[d]	96.1	685	0.32	0.23	2.69
100 °C[d]	99.0	688	0.39	0.24	2.61
110 °C[d]	99.9	1130	0.63	0.37	4.06
120 °C[d]	97.2	1145	0.68	0.32	3.51
130 °C[d]	99.1	956	0.62	0.30	3.60
140 °C[d]	95.6	804	0.42	0.26	3.17
150 °C[d]	93.7	598	0.38	0.20	2.33
160 °C[d]	95.9	332	0.43	0.10	3.57
1 h[e]	95.7	925	0.58	0.29	2.81
5 h[e]	97.2	1145	0.68	0.32	3.51
16 h[e]	89.9	1022	0.61	0.31	2.37
0 MPa[f]	94.7	521	0.51	0.17	2.38
1 MPa[f]	87.2	914	0.66	0.29	2.61
2 MPa[f]	89.9	1022	0.61	0.31	2.37
PTPA-Cl[g]	99.2	853	0.46	0.29	2.02
101 °C toluene[h]	<1	N.A.	N.A.	N.A.	N.A.
150 °C toluene[h]	65.3	256	0.34	0.06	N.A.
170 °C toluene[h]	85.6	361	0.39	0.08	N.A.
200 °C toluene[h]	95.3	610	0.41	0.18	N.A.
CMP-1 (ref. 14)	N.A.	834	0.53	N.A.	N.A.
CTF-1 (ref. 20)	N.A.	791	0.40	N.A.	N.A.
MOF-1 (ref. 21)	N.A.	516	0.29	N.A.	0.86
COF-1 (ref. 22)	N.A.	711	0.32	N.A.	N.A.

[a] Specific surface area calculated from the N_2 adsorption isotherm using the BET method. [b] The total pore volume calculated from the desorption branch of the N_2 isotherm at 77 K using the NL-DFT method. [c] CO_2 uptake at 273 K, 1 atm. [d] Reactions were performed with a reaction time of 5 h under protection of 2 MPa of N_2 by using THF as the solvent. [e] Reactions were performed with a reaction temperature of 120 °C under protection of 2 MPa of N_2, using THF as the solvent. [f] Reactions were performed with a reaction temperature of 120 °C and a reaction time of 16 h by using THF as the solvent. [g] Reactions were performed with a reaction temperature of 120 °C and a reaction time of 5 h under protection of 2 MPa of N_2 by using THF as the solvent. [h] Reactions were performed with a reaction time of 5 h under protection of 2 MPa of N_2.

$m^2\ g^{-1}$ through an additional increase of the reaction temperature to 120 °C. More importantly, the broad PSD of the PTPA with low pore volume of 0.046 $cm^3\ g^{-1}$ (control, Fig. 2(E)) was impressively tuned to be covalent organic framework (COF)-like as shown in Fig. 2(E) and S5(b and c),† with well-ordered pore sizes centered at *ca.* 7.0 Å and pore volumes reaching *ca.* 0.68 $cm^3\ g^{-1}$ (Table 1) in these FZU-PTPAs. The obtained values for the FZU-PTPAs compared favorably to previously studied BXJ-based materials (with added salts),[13] suggesting optimized conditions (and thus properties) in the CMPs when applying the FZU approach.

To understand these unprecedented outcomes of our approach, we closely investigated the solid-state ultraviolet–visible–near-infrared spectroscopy (SS UV/Vis NIR), thermogravimetric analysis (TGA), and scanning electron microscopy (SEM) of the products from our FZU procedure.[23] As shown in the SS UV/Vis NIR results (Fig. S6(a)†), a typical peak ascribed to PANi units (in the emeraldine base (EB) state) at *ca.* 600 nm in the conventionally produced PTPA showed a significant bathochromic shift in our FZU-PTPAs to 620 nm; these shifts followed the positive change in the specific surface area, proving the positive relationship between the conjugation length (thus the polymerization degree) and the surface area (as shown in Table S1†).[24,25] The TGA and derivative thermogravimetric (DTGA) analyses (Fig. S4(a) and (b),† respectively) demonstrated high thermal stability and char yields of 65–80 wt% at 800 °C under N_2, indicating a high degree of polymerization achieved *via* this facile synthetic approach. Notably, the FZU-optimized PTPAs exhibited improved thermal stability, with degradation temperatures increasing from 408 °C to 567 °C, and samples with higher surface areas showing correspondingly higher degradation temperatures in the DTGA, further supporting the correlation between polymerization degree and thermal robustness. These results suggest that the FZU method enhances the porosity and physical properties of CMPs by promoting more effective polymerization. Specifically, higher reaction temperatures favour completion of the endothermic palladium-catalysed C–N coupling, leading to more effective bond formation compared with reactions conducted at lower temperatures.[26] This mechanism was also reflected in the significant changes in macroscopic features, as shown in the SEM images (Fig. 2(F)). The original PTPA showed a compact,

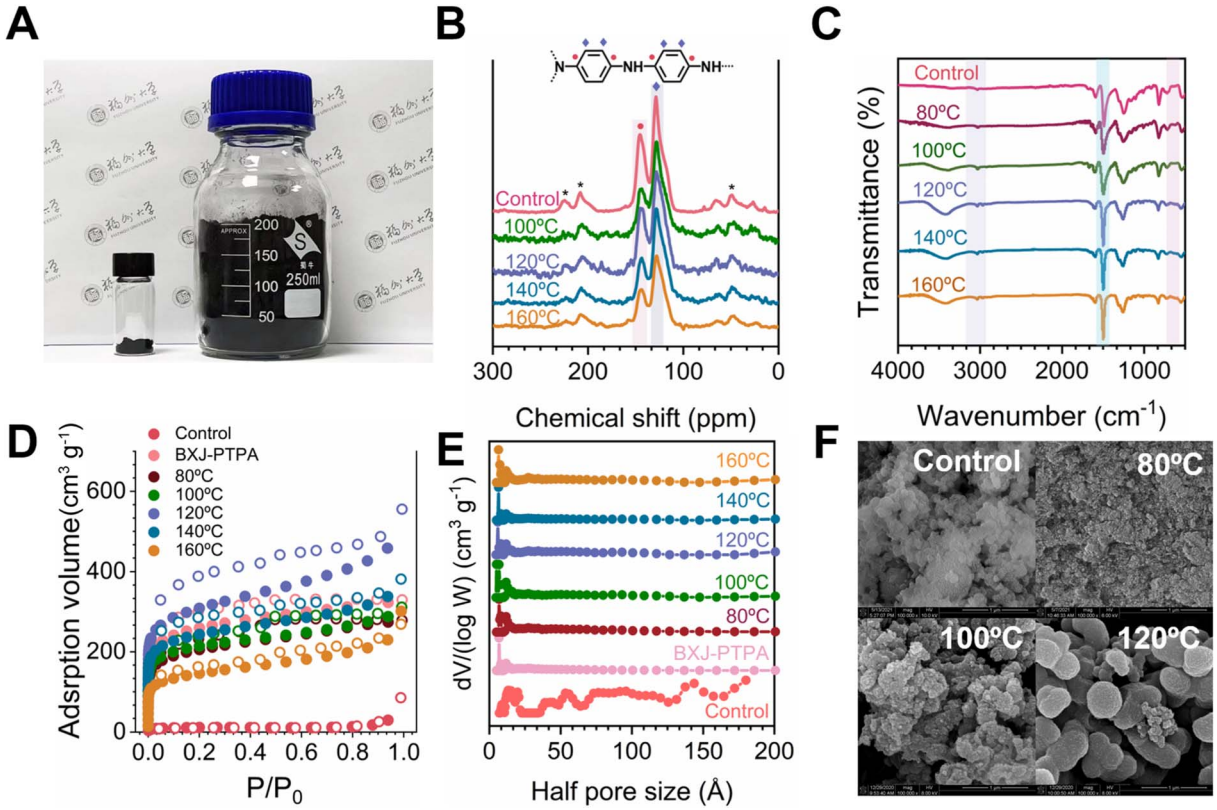

Fig. 2 (A) The products produced by the conventional (left) and FZU approach (right) at 72 h; (B) SS ^{13}C NMR spectra, (C) FTIR spectra, (D) N_2 sorption isotherms, (E) pore size distribution (PSD), and (F) SEM images of the control PTPA FZU approach at different reaction temperatures.

non-porous morphology and thus a very moderate specific surface area. However, with increase of the reaction temperature under hydrothermal conditions, these compact solids gradually turned into regular spheres, with large particle size and some small seed-like protuberances on the surface when the temperature was further increased to 120 °C. These results again suggested a homogenous and high degree of polymerization using our FZU approach, thus yielding a totally different porosity and morphology for PTPA when compared with those acquired from conventional and BXJ approaches (Fig. S21†).[13]

On reducing the reaction time to 1 h, excellent yields of 95.7% were still obtained, with identical FTIR and SS ^{13}C NMR spectra shown in Fig. S6 and S7.† Slightly lower values for the specific surface area (925 $m^2\ g^{-1}$ *vs.* 1145 $m^2\ g^{-1}$), and pore volumes (0.58 $cm^3\ g^{-1}$ *vs.* 0.68 $cm^3\ g^{-1}$) were obtained when compared with products obtained after 5 h synthesis (Fig. S8† and Table 1). Such significantly shorter reaction times, with little loss of desirable properties, make the FZU route very attractive for large-scale, greener production.

In addition to these advantages, the attractive absence of any degassing procedures was further explored. Exploring reactions performed at 120 °C, we increased the overall pressure (and thus reduced the partial pressures of oxygen and moisture) by the addition of N_2 to the autoclave. No obvious changes were observed in molecular structure (from FTIR & SS ^{13}C NMR spectra in Fig. S13 and S7†) and the yield (shown in Table 1) when comparing reactions at 0, 1 or 2 MPa N_2 over-pressure, demonstrating the success of our strategy. A ~50% reduction of the specific surface area, from 1022 $m^2\ g^{-1}$ to 521 $m^2\ g^{-1}$ (Table 1), was found when no further N_2 was added. Even so, the porosity of FZU-PTPA without any N_2 protection was ten times higher than that of conventionally acquired PTPA, again validating the success of our FZU methodology.

We have shown the positive relationship between the reaction temperature, polymerization degree and porosities. Additionally, it has been observed that the reactivity of B–H chemistry in a Schlenk tube is lower when compared with other reactions (for example, syntheses using B–H chemistry typically require 48 h or more, while CMP-1 synthesis using Sonogashira–Hagihara couplings could be acquired within seconds), which was one of the main reasons for the low polymerization degrees and porosities for the conventionally produced PTPA.[13,15] We proposed that the mechanism of our FZU approach was to enhance the B–H reactivity of aryl halides through improving the reaction temperature in the palladium-based catalytic endothermic reaction. To verify this hypothesis, we explored the synthesis of a PTPA analogue (denoted as PTPA-Cl) by using 1,4-dichlorobenzene, which showed very low reactivity in the palladium-based catalytic process.[15,27] This reaction, which should theoretically yield the same topology as PTPA, could not be achieved by the conventional or BXJ route; heating to 67 °C yielded no products in these systems due to the extremely low reactivity of 1,4–dichlorobenzene.[27] Encouragingly, our approach (120 °C, 5 h, 2 MPa additional N_2), for the

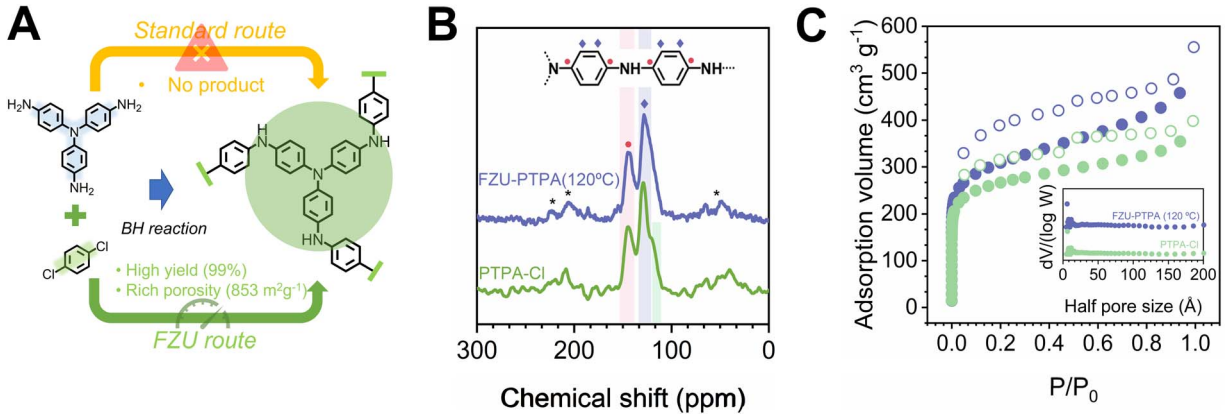

Fig. 3 Synthesis and characterization of PTPA-Cl using 1,4-dichlorobenzene as a starting monomer: (A) standard and FZU synthesis routes; (B) SS ^{13}C NMR spectra, (C) N_2 sorption isotherm and (inset) PSDs of the FZU-PTPA (120 °C) and PTPA-Cl.

first time, provided an almost quantitative yield (99.2%, Table 1), and a (nearly) identical chemical structure to the FZU-PTPA, as confirmed by the SS ^{13}C NMR and FTIR shown in Fig. 3 and S14.†[28,29] Moreover, a very promising porosity, with well-ordered PSD, high specific surface area reaching 853 $m^2\ g^{-1}$, well-defined micropores, and pore volume reaching 0.46 $cm^3\ g^{-1}$ (Table 1 and Fig. 3(C)) were acquired, suggesting that the inert 1,4-dichlorobenzene could be activated for reaction through our FZU methodology to produce structure-optimized PTPAs. This encouraging result also showed that our FZU approach could allow a wider variety of building blocks to be exploited in B–H coupling reactions compared with the standard (Schlenk tube) reaction, which marks a great opportunity to expand the applicability of B–H couplings in wider coupling chemistry.

This hypothesis could be furthermore validated by investigations to over-tune reactivity by further increasing the reaction temperature from 120 °C to 160 °C. Similar to before, the increased temperature did not change the chemical structure and the yield (as confirmed by SS ^{13}C NMR and FTIR, Fig. 2(A, B) and Table 1), but did decrease the porosity of the PTPA (shown in Table 1), with the specific surface area gradually reduced from the maximum 1145 $m^2\ g^{-1}$ at 120 °C to 332 $m^2\ g^{-1}$ at 160 °C. In addition, as it can be seen from the SEM images in Fig. S22,† a distortion in the spherical morphology occurred with increased temperature, and rod-like particles became gradually abundant, while their size decreased. These results suggested the ability to over-tune and control our FZU polymerization approach, as shown and discussed in Fig. S23–S25.†[30–32] This control over the polymerization leads to the decreased conjugation length and cross-linking, as visualized by the SS UV/Vis NIR shown in Table S1† and the thermal stability shown in Fig. S4,† finally leading to a decrease in porosity.

In addition to the excellent carbon dioxide (CO_2) uptake capabilities of our FZU PTPAs up to 4.06 mmol g^{-1} (as listed in Table 1), we explored their practical applicability and usefulness as platform for adsorption of heavy metal ions for wastewater treatment. Our FZU-PTPA exhibited exceptional CO_2 uptake capacity, achieving 4.06 mmol g^{-1} (17.8 wt%, as noted in Table 1 and Fig. 4(A)), representing a remarkable 450% increase from the 0.90 mmol g^{-1} achieved by PTPA synthesized *via* conventional methods. Notably, the isosteric heat of adsorption (Q_{st}) rose by 44%, ranging from 28.9 kJ mol^{-1} to 30.1 kJ mol^{-1} across the entire coverage range (Fig. S34†), which is superior to the values reported for most porous organic polymers (Table S3†). Notably, our FZU-PTPA showed excellent Hg(II) adsorption capability, allowing effective and exceptionally selective adsorption. As shown in Fig. 4(B), FZU-PTPAs attained 94.1% of the adsorption equilibrium within 120 s, and 99.4% within 10 min when treating water contaminated with 200 mg L^{-1} of Hg(II). These results translated to a very promising initial adsorption rate h ($k_2 q_e^2$) as high as 1203 mg g^{-1} min^{-1} (acquired from the pseudo second-order model; Fig. S30, S31 and Table S5†),[46,58] far surpassing that of other reported materials, as shown in Table S6.† For example, these values were approximately nine times higher than that of the benchmark thiol-modified COF–S–SH (143 mg g^{-1} min^{-1}).[59] The outstanding performance of our FZU-PTPA for mercury removal was further confirmed by its extraordinary adsorption capacity (Fig. 4(B)), with a maximum capacity reaching 1111 mg g^{-1} at 25 °C as fitted by the Langmuir model (Fig. S32, S33 and Table S7†).[60] This unparalleled capacity could be further improved to 1429 mg g^{-1} by slightly increasing the temperature to 45 °C (showing ΔH = 27.16 kJ mol^{-1} and ΔG = −5.96 kJ mol^{-1} as depicted in Fig. S34 and Table S9†), outperforming all reported materials including PAF–1–SH (1014 mg g^{-1})[55] and TAPB–BMTTPA–COF (734 mg g^{-1})[61] (Table S10†). Based on the excellent Hg adsorption performance of FZU-PTPA, particularly its removal efficiency of nearly 100% for Hg(II) at low concentrations, further experiments in multi-ion coexisting solutions demonstrated the simultaneous affinity and selectivity of FZU-PTPA for Hg(II). FZU-PTPA demonstrated an impressive selectivity of 98% for Hg(II), as illustrated in Fig. 4(B). The ion-dependent affinity exhibited by FZU-PTPA results in selectivity coefficients for Hg(II) ranging from 140 to 90 000 against other cations (Fig. S35†). Achieving such exclusive selectivity for specific metal ions is a challenge, with surface functionalization of ion-imprinted polymers emerging as a prominent strategy. Selectivity is achieved through the precise engineering of recognition cavities or sites, which are designed to retain the

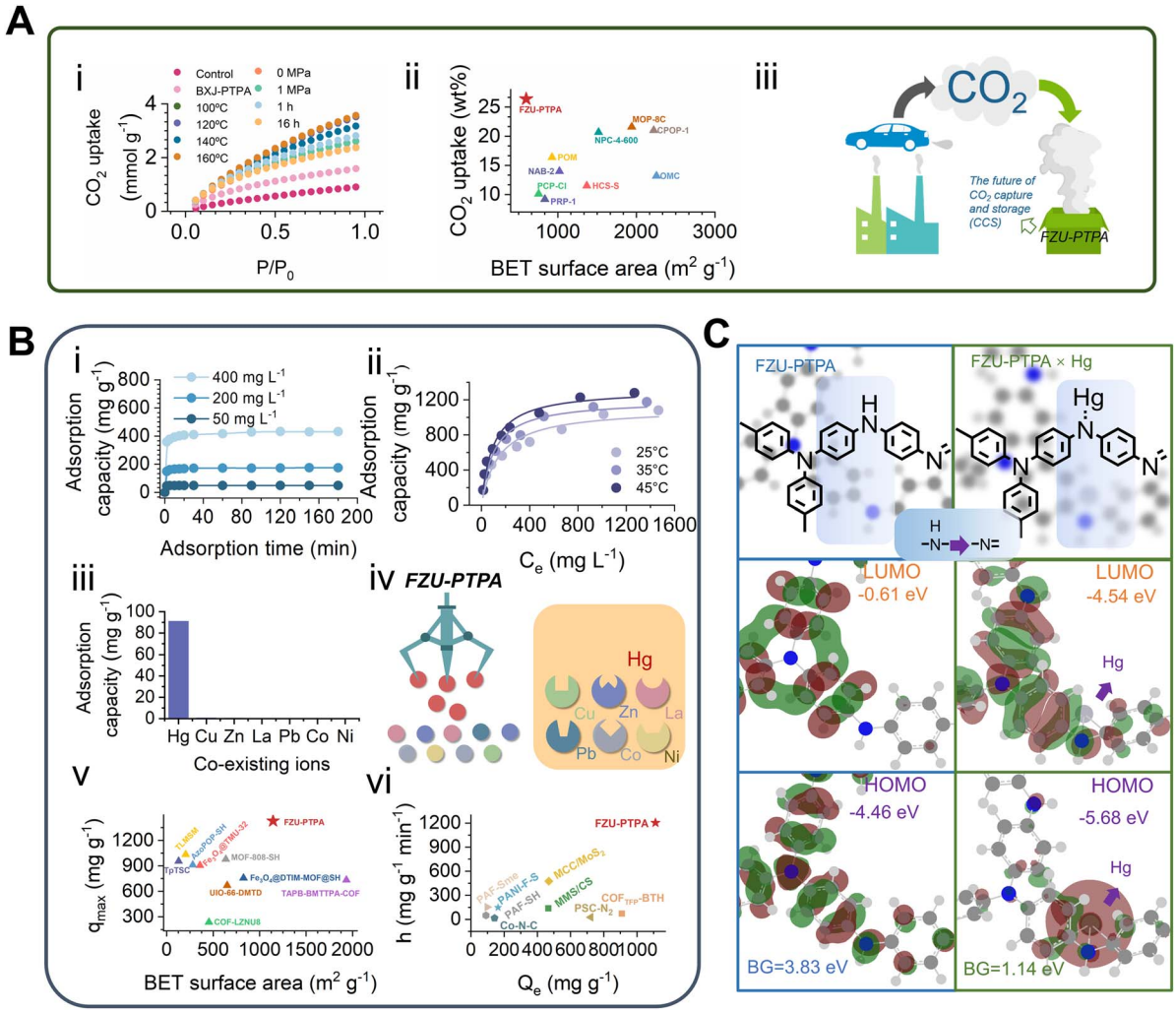

Fig. 4 (A) Gas adsorption performance of the FZU-PTPA: (i) CO_2 adsorption capacity at 273 K; (ii) the rank of our FZU-PTPA among the reported materials (red star);[33–37] (iii) the future of the carbon capture and storage (CCS) using our FZU-PTPA. (B) Mercury adsorption performance of the FZU-PTPA: (i) kinetic data for mercury at various initial concentrations; (ii) isotherm data collected at different temperatures; (iii) selectivity towards ions in the initial concentration of 100 mg L^{-1} for each;[38–45] (iv) illustration of the exceptional selectivity towards mercury ion of FZU-PTPA; (v) ultra-high adsorption capacity of FZU-PTPA among other advanced materials (red star);[38–52] (vi) benchmarking our FZU-PTPA (red star) in terms of the initial adsorption rate compared with published materials;[53–57] (C) electron interaction (in HOMO and LUMO) between FZU-PTPA and Hg(II).

three-dimensional (3D) structures of the target ions.[62] However, the preparation process is complex and influenced by various factors during polymerization and the subsequent removal of the template ion. Our method offers a straightforward alternative for the selective adsorption isolation of ions compared to ion-imprinted polymers. By synthesizing high porosity FZU-PTPA using a scalable autoclaving process, we enhance the accessibility of the adsorption sites. Moreover, the FZU-PTPA maintained over 90% of its original removal efficiency for Hg(II) across five consecutive cycles, demonstrating its ability to retain structural integrity and the ability to effectively remove Hg(II) from complex mixtures, even after multiple treatments with strong acids.

These encouraging results towards Hg(II) adsorption, as illustrated in Fig. 4(C), were facilitated by the presence of –NH– moieties throughout the framework structure. These interactions were verified by FTIR (Fig. S37†) and X-ray photoelectron spectroscopy (XPS) investigations (Fig. S54–S56 and Table S23†), in which the benzenoid amine (–NH–) was diminished after interaction with Hg(II). Density functional theory (DFT) calculations in Fig. 4(C) show a strong charge-–transfer interaction between FZU-PTPA and Hg(II) through –NH–, resulting in the extensive reduction of the lowest unoccupied molecular orbital (LUMO) level of PTPA. In addition, the newly formed microporous structures and uniformly dispersed sphere morphology (shown in Fig. 2(F)) further facilitated ion diffusion and NH–metal ion contact. In contrast, the conventionally synthesized and BXJ-produced PTPAs showed similar chemical structure but much lower adsorption capacity, resulting from the poor porosity or the aggregated particle morphology that hinder the adsorption of Hg(II) on the –NH– adsorption sites.

Conclusions

In conclusion, our new synthetic FZU approach enables the large-scale production of palladium-catalysed CMPs, through an ultra-efficient one-step reaction, extremely short reaction time, no degassing requirements, and widely applicable products. Carefully selected (temperature) conditions provide an important route to improve the reactivity of aryl halides in B–H coupling chemistry, yielding CMPs with dramatically improved physical properties, including high specific surface areas and optimized, well-ordered micropores. FZU-PTPAs demonstrate exceptional adsorption capabilities for CO_2 and heavy metal ions, achieving impressive capacities reaching up to 4.06 mmol g^{-1} for CO_2 and 1429 mg g^{-1} for Hg(II), and exhibiting high efficiency and selectivity. Notably, the Hg(II) uptake of our cross-linked microporous polymers is the highest compared with other porous organic polymer systems. These advances now make this class of CMPs an appealing platform to address significant global environmental challenges, and worthy of further exploration. We expect real-world applications in the very near future.

Data availability

All data generated or analysed during this investigation are included in this manuscript and ESI.† The data that support the findings of this study are available on request from the corresponding author, tingqiu@fzu.edu.cn, charl.faul@bristol.ac.uk, jiechen@fzu.edu.cn, upon reasonable request.

Author contributions

Conceptualization, D. T., Z. X. and J. C.; data curation, J. W. and Z. X.; formal analysis, D. T. and J. W.; methodology, D.T. Z. X., and J. W.; project administration, T. Q. and J. C.; supervision, T. Q, J. C., C. F.; writing—original draft preparation, Z. X. and J. C.; writing—review and editing, D. T., T. Q., C. F. and J. C.; visualization, J. W., T. Q. and J. C.; funding acquisition, T. Q., and J. C.

Conflicts of interest

The authors declare no competing interests.

Acknowledgements

This work was supported by the National Natural Science Foundation of China (Grant No. 22478077, 22278077). We also greatly acknowledge support from State Key Laboratory of Green and Efficient Development of Phosphorus Resources. J. D. W. thanks the Engineering and Physical Science Research Council through the EPSRC Centre for Doctoral Training in Composites Science, Engineering and Manufacturing [EP/S021728/1].

References

1 Y. Su, B. Li, Z. Wang, A. Legrand, T. Aoyama, S. Fu, Y. Wu, K.-I. Otake, M. Bonn, H. I. Wang, Q. Liao, K. Urayama, S. Kitagawa, L. Huang, S. Furukawa and C. Gu, *J. Am. Chem. Soc.*, 2024, **146**, 15479–15487.
2 S. Wang, Z. Xie, D. Zhu, S. Fu, Y. Wu, H. Yu, C. Lu, P. Zhou, M. Bonn, H. I. Wang, Q. Liao, H. Xu, X. Chen and C. Gu, *Nat. Commun.*, 2023, **14**, 6891.
3 Y. Su, B. Li, H. Xu, C. Lu, S. Wang, B. Chen, Z. Wang, W. Wang, K.-I. Otake, S. Kitagawa, L. Huang and C. Gu, *J. Am. Chem. Soc.*, 2022, **144**, 18218–18222.
4 J. M. Lee and A. I. Cooper, *Chem. Rev.*, 2020, **120**, 2171–2214.
5 J. Zhu, X. Lou, Y. Wang, Z. Xiong, J. Chen and W. Yan, *Chem. Eng. Sci.*, 2022, **248**, 117119.
6 X. Lou, X. Chen, D. Tang, Q. Wang, Y. Tian, M. Tu, Y. Wang, C. Ye, J. Chen and T. Qiu, *Langmuir*, 2022, **38**, 13238–13247.
7 Y. Liao, S. Cai, S. Huang, X. Wang and C. F. J. Faul, *Macromol. Rapid Commun.*, 2014, **35**, 1833–1839.
8 Y. Liao, J. Weber, B. M. Mills, Z. Ren and C. F. J. Faul, *Macromolecules*, 2016, **49**, 6322–6333.
9 X. Chen, Y. Wang, J. Wang, J. Liu, S. Sun, L. Zhu, Q. Ma, N. Zhu, X. Wang, J. Chen and W. Yan, *J. Mater. Chem. A*, 2022, **10**, 1359–1368.
10 D. Zhang, Q. Chen, C. Shi, M. Chen, K. Ma, J. Wan and R. Liu, *Adv. Funct. Mater.*, 2020, **31**, 2003619.
11 H. Ali, O. Iqbal, M. Sadiq, Y. Cheng, X. Yan, B. Al Alwan, A. El Jery, H. U. Rahman, Y. Qian, A. Hayat, D. Yue and Z. Ajmal, *Nano Mater. Sci.*, 2025, DOI: 10.1016/j.nanoms.2024.08.008.
12 Y. Liao, J. Weber and C. F. J. Faul, *Chem. Commun.*, 2014, **50**, 8002–8005.
13 Y. Li, Q. Chen, T. Xu, Z. Xie, J. Liu, X. Yu, S. Ma, T. Qin and L. Chen, *J. Am. Chem. Soc.*, 2019, **141**, 13822–13828.
14 J.-X. Jiang, F. Su, A. Trewin, C. D. Wood, N. L. Campbell, H. Niu, C. Dickinson, A. Y. Ganin, M. J. Rosseinsky, Y. Z. Khimyak and A. I. Cooper, *Angew. Chem., Int. Ed.*, 2007, **46**, 8574–8578.
15 J.-X. Jiang, F. Su, A. Trewin, C. D. Wood, H. Niu, J. T. A. Jones, Y. Z. Khimyak and A. I. Cooper, *J. Am. Chem. Soc.*, 2008, **130**, 7710–7720.
16 K. Amin, B. C. Baker, L. Pan, W. Mehmood, Z. Hao, R. Nawaz, Z. Wei and C. F. J. Faul, *Adv. Mater.*, 2025, **37**, 2410262.
17 W. Lyu, W. Zhang, H. Liu, Y. Liu, H. Zuo, C. Yan, C. F. J. Faul, A. Thomas, M. Zhu and Y. Liao, *Chem. Mater.*, 2020, **32**, 8276–8285.
18 J. Chen, N. Wang, Y. Liu, J. Zhu, J. Feng and W. Yan, *Synth. Met.*, 2018, **245**, 32–41.
19 H. Zhang, L. Zhong, J. Xie, F. Yang, X. Liu and X. Lu, *Adv. Mater.*, 2021, **33**, 2101857.
20 P. Kuhn, M. Antonietti and A. Thomas, *Angew. Chem., Int. Ed.*, 2008, **47**, 3450–3453.
21 Z. Guo, H. Xu, S. Su, J. Cai, S. Dang, S. Xiang, G. Qian, H. Zhang, M. O'Keeffe and B. Chen, *Chem. Commun.*, 2011, **47**, 5551–5553.
22 A. P. Côté, A. I. Benin, N. W. Ockwig, M. O'Keeffe, A. J. Matzger and O. M. Yaghi, *Science*, 2005, **310**, 1166–1170.

23 B. P. Fors and S. L. Buchwald, *J. Am. Chem. Soc.*, 2010, **132**, 15914–15917.
24 J. Stejskal, M. Trchová, P. Bober, P. Humpolíček, V. Kašpárková, I. Sapurina, M. A. Shishov and M. Varga, *Encycl. Polym. Sci. Technol.*, 2015, **46**, 1–44.
25 E. T. Kang, K. G. Neoh and K. L. Tan, *Prog. Polym. Sci.*, 1998, **23**, 277–324.
26 S. Liu, Z. Jin, Y. C. Teo and Y. Xia, *J. Am. Chem. Soc.*, 2014, **136**, 17434–17437.
27 A. F. Littke and G. C. Fu, *Angew. Chem., Int. Ed.*, 2002, **41**, 4176–4211.
28 N. Graf, E. Yegen, T. Gross, A. Lippitz, W. Weigel, S. Krakert, A. Terfort and W. E. S. Unger, *Surf. Sci.*, 2009, **603**, 2849–2860.
29 S. Golczak, A. Kanciurzewska, M. Fahlman, K. Langer and J. J. Langer, *Solid State Ionics*, 2008, **179**, 2234–2239.
30 P. N. Adams, P. J. Laughlin, A. P. Monkman and A. M. Kenwright, *Polymer*, 1996, **37**, 3411–3417.
31 A. Ohtani, M. Abe, M. Ezoe, T. Doi, T. Miyata and A. Miyake, *Synth. Met.*, 1993, **57**, 3696–3701.
32 P. N. Adams and A. P. Monkman, *Synth. Met.*, 1997, **87**, 165–169.
33 J. Wang, W. K. Sng, G. Yi and Y. Zhang, *Chem. Commun.*, 2015, **51**, 12076–12079.
34 O. Buyukcakir, S. H. Je, D. S. Choi, S. N. Talapaneni, Y. Seo, Y. Jung, K. Polychronopoulou and A. Coskun, *Chem. Commun.*, 2016, **52**, 934–937.
35 O. Buyukcakir, S. H. Je, J. Park, H. A. Patel, Y. Jung, C. T. Yavuz and A. Coskun, *Chemistry*, 2015, **21**, 15320–15327.
36 X. Hu, H. Wang, C. F. J. Faul, J. Wen, Y. Wei, M. Zhu and Y. Liao, *Chem. Eng. J.*, 2020, **382**, 122998.
37 X. Li, S. Bai, Z. Zhu, J. Sun, X. Jin, X. Wu and J. Liu, *Langmuir*, 2017, **33**, 1248–1255.
38 S. Y. Ding, M. Dong, Y. W. Wang, Y. T. Chen, H. Z. Wang, C. Y. Su and W. Wang, *J. Am. Chem. Soc.*, 2016, **138**, 3031–3037.
39 C. Tang, Y. Qin, C. Ni and J. Zou, *ACS App. Polym. Mater.*, 2022, **4**, 849–858.
40 Y. Li, M. Tan, G. Liu, D. Si, N. Chen and D. Zhou, *J. Mater. Chem. A*, 2022, **10**, 6724–6730.
41 N. Abdollahi, S. A. Akbar Razavi, A. Morsali and M. L. Hu, *J. Hazard. Mater.*, 2020, **387**, 121667.
42 C. Ji, Y. Ren, H. Yu, M. Hua, L. Lv and W. Zhang, *Chem. Eng. J.*, 2022, **430**, 132960.
43 N. Abdollahi, S. A. Akbar Razavi, A. Morsali and M.-L. Hu, *J. Hazard. Mater.*, 2020, **387**, 121667.
44 C. Xiong, X. Zhang, K. Liang, C. Wu, W. Wu, X. Rao and Q. Chen, *ACS Appl. Mater. Interfaces*, 2025, **17**, 13970–13979.
45 L. Fu, S. Wang, G. Lin, L. Zhang, Q. Liu, J. Fang, C. Wei and G. Liu, *J. Hazard. Mater.*, 2019, **368**, 42–51.
46 L. S. Blankenship, N. Balahmar and R. Mokaya, *Nat. Commun.*, 2017, **8**, 1545.
47 L. S. Blankenship and R. Mokaya, *Energy Environ. Sci.*, 2017, **10**, 2552–2562.
48 A. P. Pandey, A. Bhatnagar, V. Shukla, P. K. Soni, S. Singh, S. K. Verma, M. Shaneeth, V. Sekkar and O. N. Srivastava, *Int. Hydrogen Energy*, 2020, **45**, 30818–30827.
49 O. K. Farha, A. Özgür Yazaydın, I. Eryazici, C. D. Malliakas, B. G. Hauser, M. G. Kanatzidis, S. T. Nguyen, R. Q. Snurr and J. T. Hupp, *Nat. Chem.*, 2010, **2**, 944–948.
50 S. Barman, A. Khutia, R. Koitz, O. Blacque, H. Furukawa, M. Iannuzzi, O. M. Yaghi, C. Janiak, J. Hutter and H. Berke, *J. Mater. Chem. A*, 2014, **2**, 18823–18830.
51 L. Morris, J. J. Hales, M. L. Trudeau, P. Georgiev, J. P. Embs, J. Eckert, N. Kaltsoyannis and D. M. Antonelli, *Energy Environ. Sci.*, 2019, **12**, 1580–1591.
52 F.-G. Li, C. Liu, D. Yuan, F. Dai, R. Wang, Z. Wang, X. Lu and D. Sun, *CCS Chem.*, 2022, **4**, 832–837.
53 P. Gao, J. Lei, J. Tan, G. Wang, H. Liu and L. Zhou, *Compos. Commun.*, 2021, **25**, 100736.
54 H. He, X. Meng, Q. Yue, W. Yin, Y. Gao, P. Fang and L. Shen, *Chem. Eng. J.*, 2021, **405**, 126743.
55 B. Li, Y. Zhang, D. Ma, Z. Shi and S. Ma, *Nat. Commun.*, 2014, **5**, 5537.
56 L. Xing, M. Li, T. Qi, L. Mao, Z. Hu, E. Zhang, G. P. Hao, B. Mao and L. Wang, *Environ. Sci. Technol.*, 2022, **56**, 4531–4541.
57 Q. Ge and H. Liu, *Chem. Eng. J.*, 2022, **428**, 132579.
58 Y. S. Ho and G. McKay, *Process Biochem.*, 1999, **34**, 451–465.
59 Q. Sun, B. Aguila, J. Perman, L. D. Earl, C. W. Abney, Y. Cheng, H. Wei, N. Nguyen, L. Wojtas and S. Ma, *J. Am. Chem. Soc.*, 2017, **139**, 2786–2793.
60 J. Chen, M. Yu, C. Wang, J. Feng and W. Yan, *Langmuir*, 2018, **34**, 10187–10196.
61 N. Huang, L. Zhai, H. Xu and D. Jiang, *J. Am. Chem. Soc.*, 2017, **139**, 2428–2434.
62 Y. Su, Z. Chen, X. Tang, H. Xu, Y. Zhang and C. Gu, *Angew. Chem., Int. Ed.*, 2021, **60**, 24424–24429.